Supporting Information for

Stable Interphase Chemistry of Textured Zn Anode for Rechargeable Aqueous Batteries

Jindi Wang[1,†], Bao Zhang[2,†], Zhao Cai[1,†], Renming Zhan[1], Wenyu Wang[1], Lin Fu[1], Mintao Wan[1], Run Xiao[1], Yangtao Ou[1], Li Wang[3], Jianjun Jiang[2], Zhi Wei Seh[4], Hong Li[5], and Yongming Sun[1,]*

1 Wuhan National Laboratory for Optoelectronics, Huazhong University of Science and Technology, Wuhan, 430074, China

2 School of Optical and Electronic Information, Huazhong University of Science and Technology, Wuhan, 430074, China

3 Institute of Nuclear & New Energy Technology, Tsinghua University, Beijing, 100084, China

4 Institute of Materials Research and Engineering, Agency for Science, Technology and Research (A*STAR), 2 Fusionopolis Way, Innovis, 138634, Singapore

5 Institute of Physics, Chinese Academy of Sciences, Beijing 100190, China

† These authors contributed equally to this work.

* Email: yongmingsun@hust.edu.cn.

Supplementary Figures

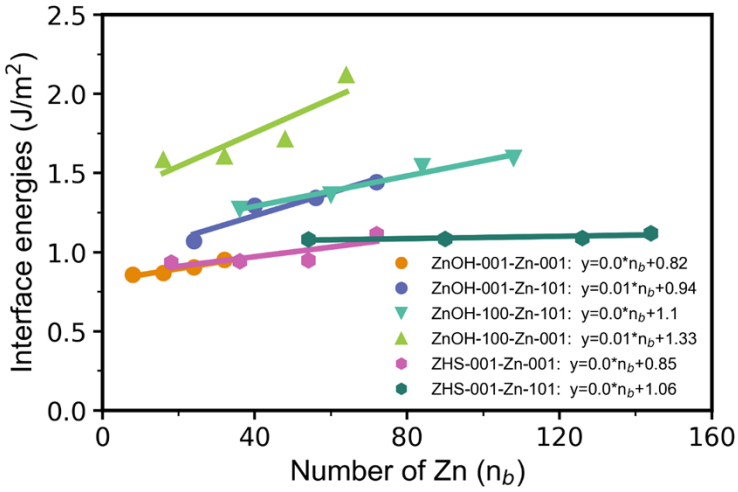

Fig. S1 Plot of the relationship between the interfacial energy for possible interfaces and the number of Zn metal formula units.

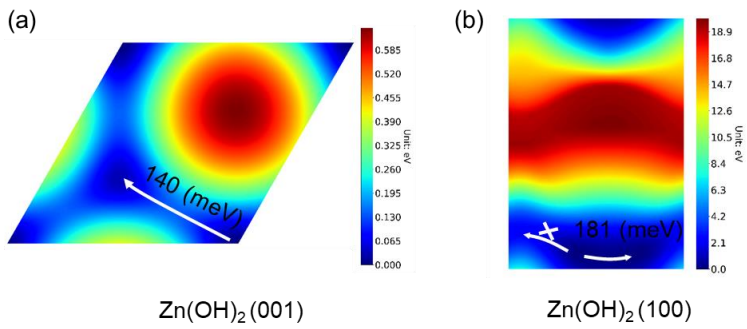

Fig. S2 Potential surface energy of (a) the (001) plane and (b) the (100) plane of $Zn(OH)_2$ based on ReaxFF method. $Zn(OH)_2$ (001) has a low surface Zn atom diffusion barrier, which is beneficial for promoting the 2D diffusion and inhibiting dendrite growth.

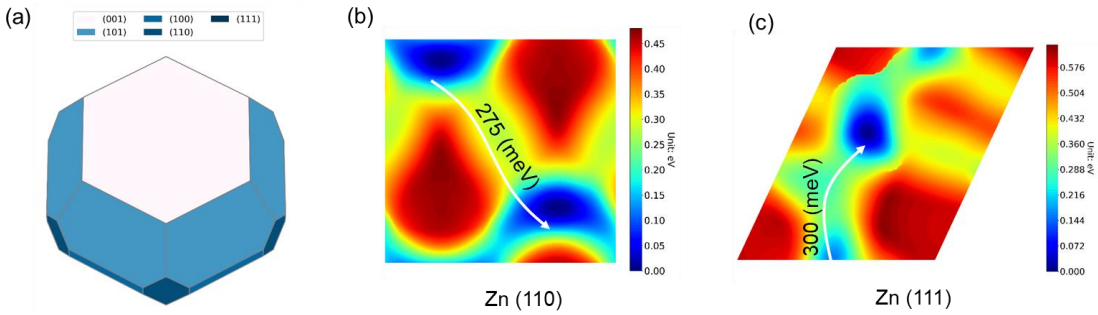

Fig. S3 Surface properties of Zn metal based on MEAM method: Wulffshape and potential surface energy of hopping mechanism.

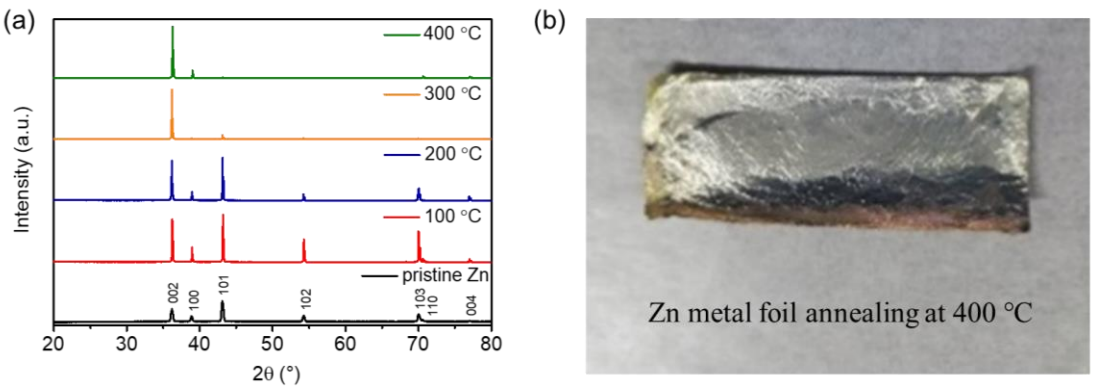

Fig. S4 (a) XRD patterns of the Zn metal foils after annealing at different temperatures and (b) digital image of the Zn metal foil after annealing at 400 °C.

To investigate the temperature independence, a wide temperature range from 100 ºC to 400 ºC was adopted for annealing of metallic Zn. The XRD results confirmed that there was no texture change for metallic Zn after annealing at 100–200 ºC. A high annealing temperature of 400 ºC caused structural damage of the Zn metal foil, since it was very close to the melting point of metallic Zn (420 ºC). In our experiment, an optimized temperature of 300 ºC was used for the fabrication of (002)-Zn electrode.

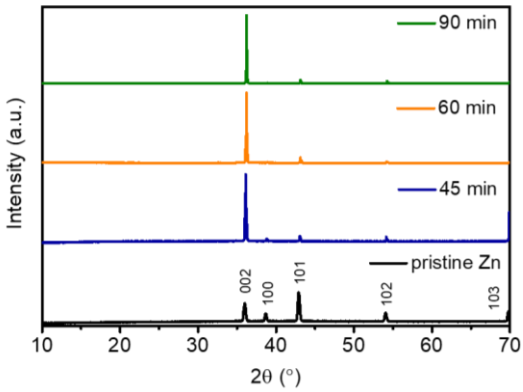

Fig. S5 XRD patterns of the Zn metal foil after annealing at 300 °C for different times.

XRD results showed that the proportion of (002) plane increased continuously for Zn metal annealing at 300 ºC with increase of annealing time from 45 to 90 min, as demonstrated by the change of texture coefficient, which reached a peak for the sample with 60 min annealing. In our experiment, an optimized annealing time of 60 min was used for the fabrication of (002)-Zn electrode.

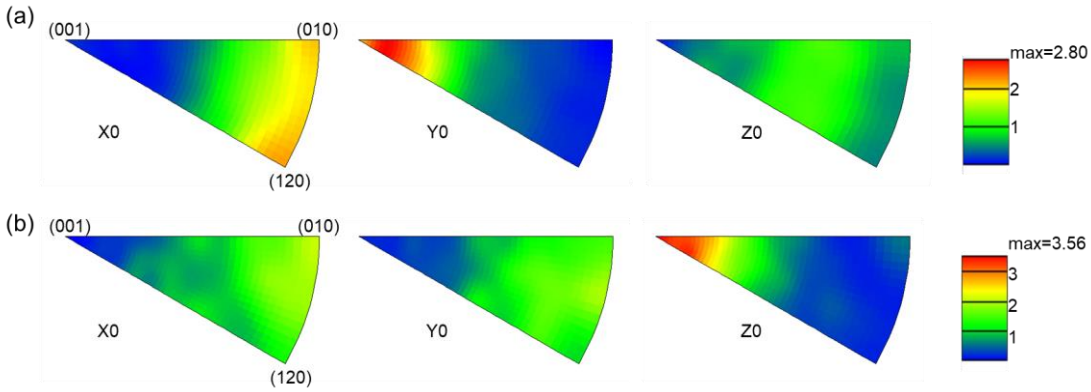

Fig. S6 EBSD reverse pole figures of the (a) pristine Zn and (b) (002)-Zn foil electrodes.

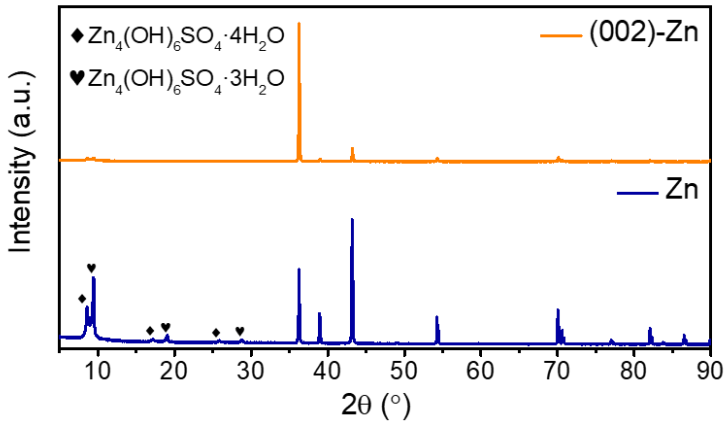

Fig. S7 XRD patterns of pristine Zn and (002)-Zn electrodes after resting in aqueous $ZnSO_4$ electrolyte for 7 days.

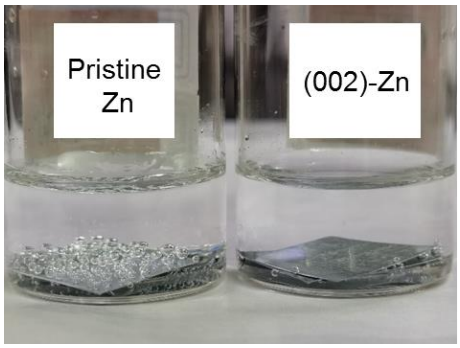

Fig. S8 Digital image of the a) pristine Zn and b) (002)-Zn foil electrodes after resting in aqueous $ZnSO_4$ electrolyte for 7 days.

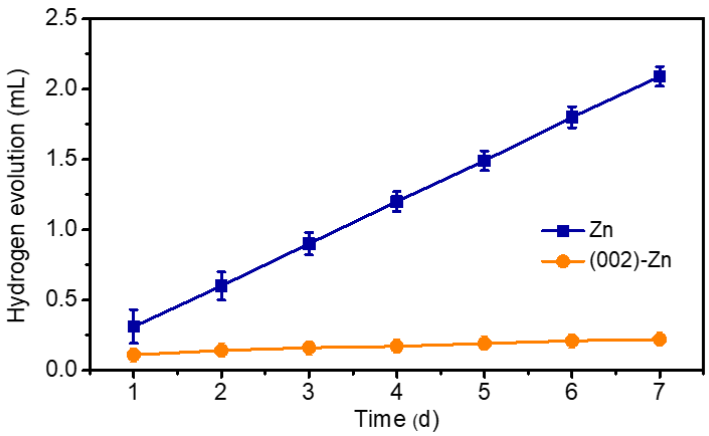

Fig. S9 The hydrogen evolution volume-time plots for the pristine Zn and (002)-Zn electrodes resting in aqueous $ZnSO_4$ electrolyte.

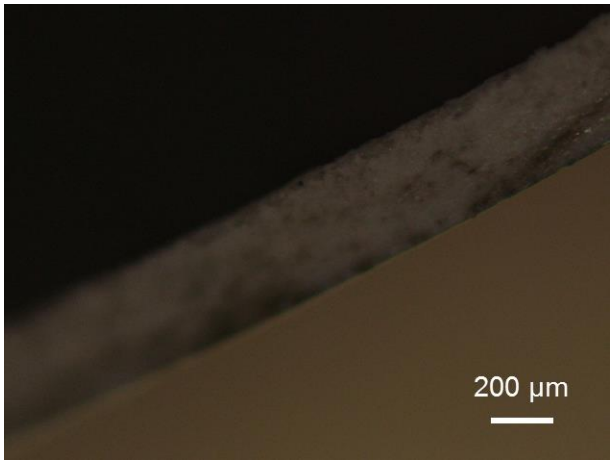

Fig. S10 Cross-section OM image of the as-prepared ZHS film for electrochemical measurements. The thickness of the ZHS film was 360 μm.

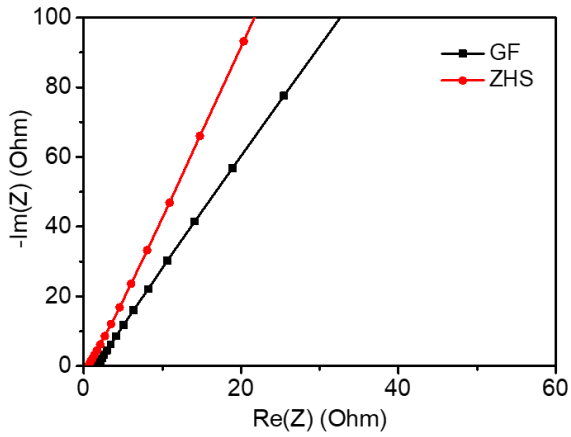

Fig. S11 The EIS results of glass fiber (GF) separator and ZHS solid electrolyte for the ionic conductivity measurement.

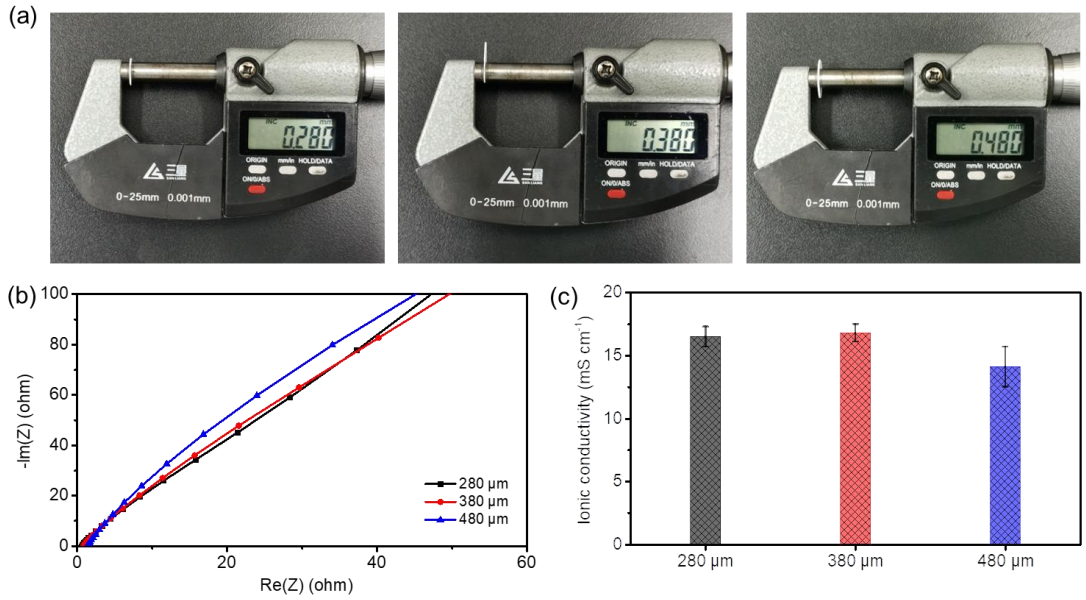

Fig. S12 (a) Digital image of the as-prepared ZHS membranes with the thickness of 280 μm, 380 μm, and 480 μm. (b) EIS results and (c) ionic conductivities of the as-prepared ZHS membranes with different thicknesses. The error bars were obtained by repeated experiments for at least 5 times.

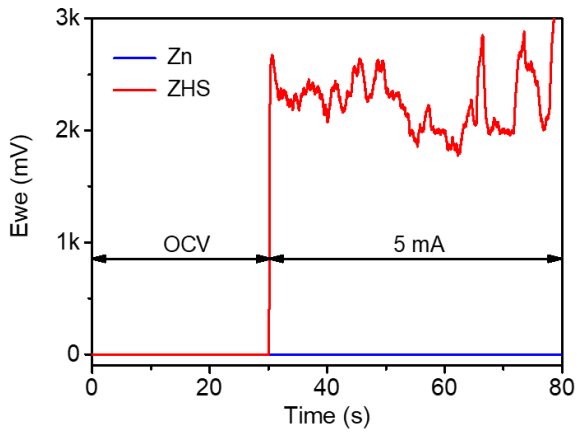

Fig. S13 Voltage response of Zn metal foil and ZHS film under an applied current density of 5 mA cm^{-2}, suggesting the high electronic resistance of ZHS.

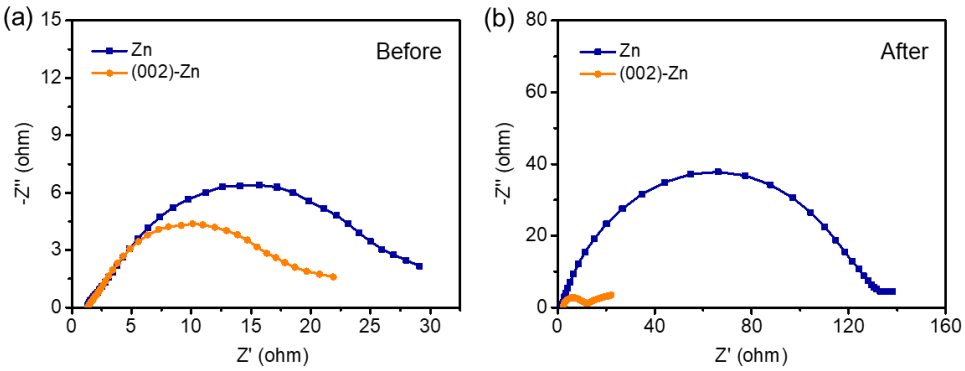

Fig. S14 EIS analysis of (a) pristine Zn and (b) (002)-Zn electrodes before and after 10 cycles at 1 mA cm^{-2} and 1 mAh cm^{-2}.

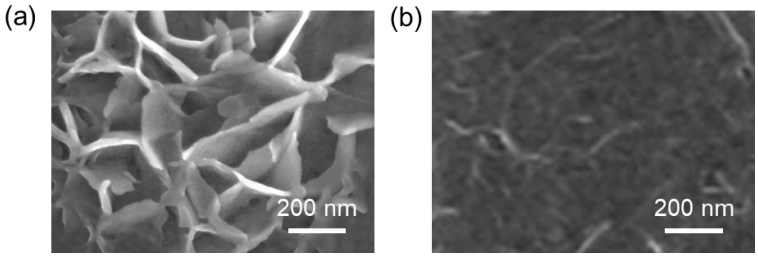

Fig. S15 High-resolution SEM images of (a) pristine Zn and (b) (002)-Zn electrodes after resting in electrolyte for 1 h after battery assembly before the deposition of Zn.

The growth of ZHS on the pristine Zn and (002)-Zn electrodes after resting in electrolyte was observed. The ZHS plates on the pristine Zn electrode were mostly vertical, while most of the ZHS plates on the (002)-Zn electrode were horizontal.

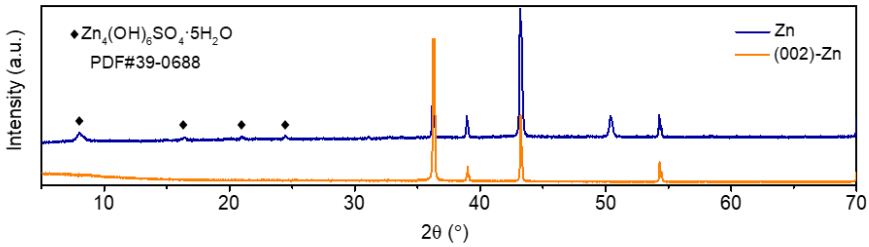

Fig. S16 XRD patterns of pristine Zn and (002)-Zn electrodes after 40 cycles at 5 mA cm^{-2} and 2 mAh cm^{-2}.

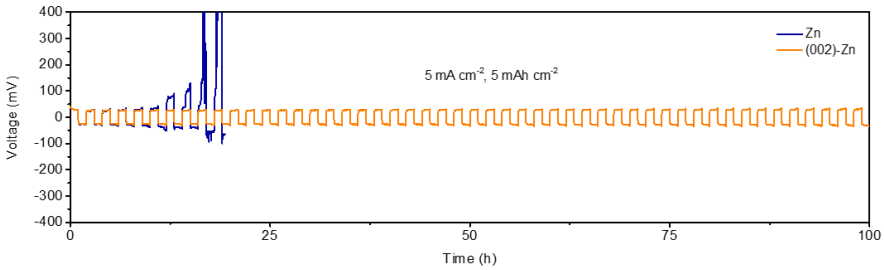

Fig. S17 Voltage profiles of Zn||Zn and (002)-Zn||(002)-Zn symmetric cells at 5 mA cm^{-2} and 5 mAh cm^{-2}.

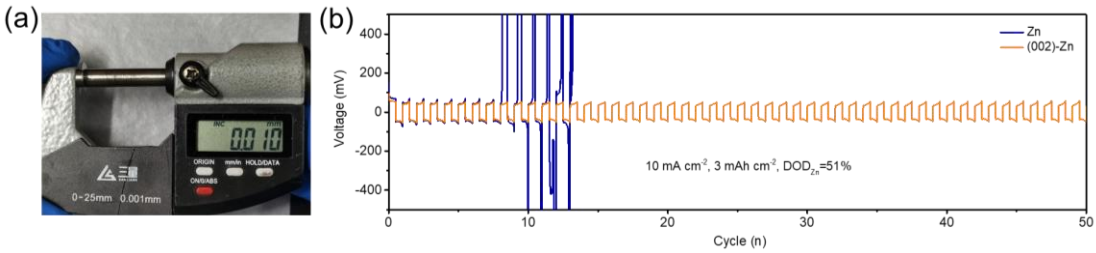

Fig. S18 (a) Digital image of the thin Zn electrode with thickness of 10 μm for symmetrical cell test. (b) Voltage profiles of Zn||Zn and (002)-Zn||(002)-Zn symmetric cells with the thin Zn electrodes cycled at 10 mA cm^{-2} and 3 mAh cm^{-2}.

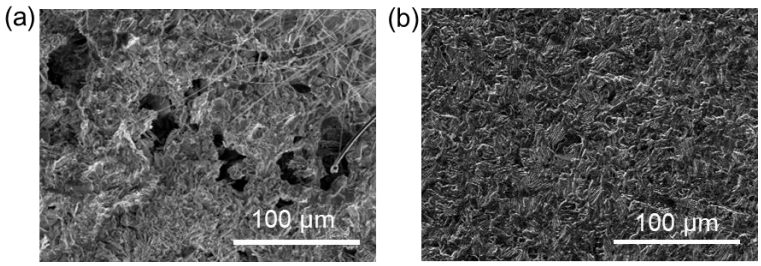

Fig. S19 (a) SEM image of the pristine Zn electrode after 100 cycles in MnO_2||pristine Zn cell under 10 *C*. (b) SEM image of (002)-Zn electrode after 1000 cycles in MnO_2||(002)-Zn cell under 10 *C*.

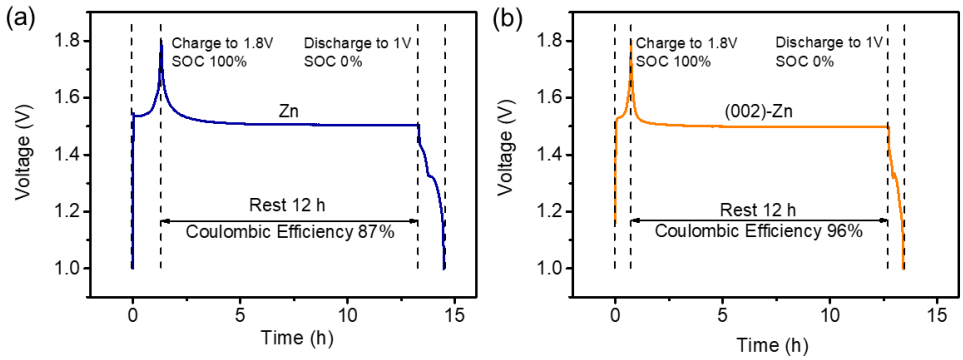

Fig. S20 The self-discharge results of (a) MnO_2||pristine Zn and (b) MnO_2||(002)-Zn cells.

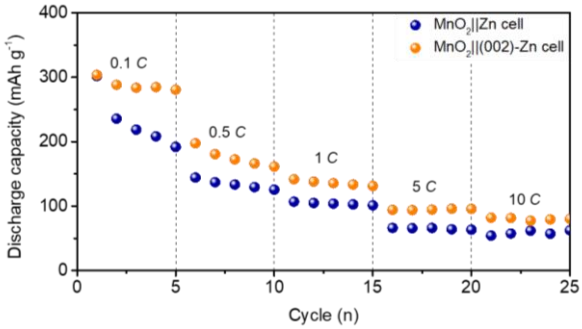

Fig. S21 Rate capability of the MnO_2||pristine Zn and MnO_2||(002)-Zn cells.

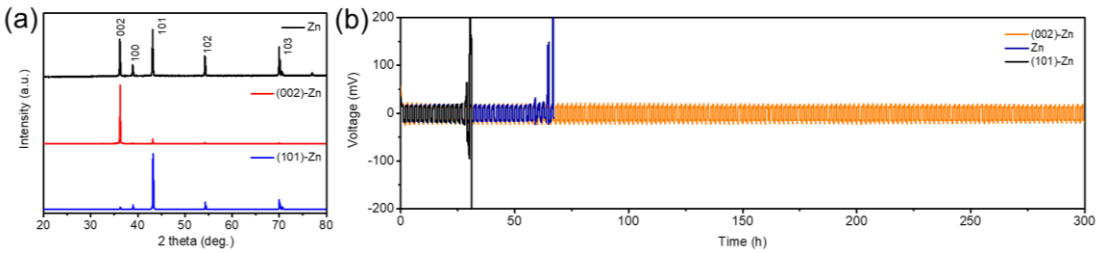

Fig. S22 (a) XRD analysis of pristine Zn, (002)-Zn, and (101)-Zn electrodes. (b) Voltage profiles of Zn||Zn, (002)-Zn||(002)-Zn, and (101)-Zn||(101)-Zn symmetric cells at 1 mA cm^{-2} and 1 mAh cm^{-2}.

After resting in aqueous $ZnSO_4$ electrolyte, ZHS formed on the three electrodes with different textures. The cycling results of these electrodes suggested that the stability of $(002)_{Zn}$-$(001)_{ZHS}$ was better than the other two electrodes.

Supplementary Tables

Table S1 The bill of material (BOM) for lithium ion batteries (LIB) and Zn metal batteries (ZMB), the unit price of materials was obtained from BatPac 4.0 and alibaba.com.

		LIB / 100 Ah			ZMB / 100 Ah		
		Materials	**Unit price / $ / kg**	**Price / $**	**Materials**	**Unit price / $ / kg**	**Price / $**
Positive 9:0.5:0.5	Active material	$LiFePO_4$ / 150 mAh g^{-1}	20.6	13.73	MnO_2 / 300 mAh g^{-1}	5	1.67
	Carbon	C	6.6	0.24	C	6.6	0.12
	Binder	PVDF	9.5	0.35	PTFE	10	0.18
	Binder solvent	NMP	3.1	2.25	H_2O	0	0
Negative 9:0.5:0.5 N/P=1.2	Active material	C / 350 mAh g^{-1}	6.6	2.26	Zn metal / 820 mAh g^{-1}	2	0.29
	Binder	CMC	20	0.14			
		SBR	4.2	0.08			
	Binder solvent	H_2O	0	0			
Positive current collector		Al foil	4.5	0.52	Ti foil	5	0.57
Negative current collector		Cu foil	14	2.58	\	\	\
Electrolyte		$LiPF_6$, DMC	15	1.27	$ZnSO_4$, H_2O	2	0.17
Average potential			3.3 V		1.4 V		
Cost			70.96 $ / kWh		21.43 $ / kWh		

Table S2 Surface properties of Zn metal based DFT calculations.

	001	**100**	**101**	**110**	**111**
Surface energies (J/m^2)	0.64	1.10	1.09	1.40	1.34
E_{diff} (meV)	20	47	269		

Table S3 Comparison of cycle life for Zn metal electrode in this work with that in recent reports.

No.	**Areal capacity**	**Current density**	**Cycle life**	**Ref.**
1	0.5 mAh cm^{-2}	0.25 mA cm^{-2}	100 h	1
2	0.5 mAh cm^{-2}	0.5 mA cm^{-2}	350 h	2
3	0.5 mAh cm^{-2}	0.5 mA cm^{-2}	700 h	3
4	0.5 mAh cm^{-2}	0.5 mA cm^{-2}	1000 h	4
5	0.5 mAh cm^{-2}	0.5 mA cm^{-2}	1800 h	5
6	0.5 mAh cm^{-2}	0.5 mA cm^{-2}	2200 h	6
7	0.5 mAh cm^{-2}	0.5 mA cm^{-2}	600 h	7
8	0.5 mAh cm^{-2}	0.5 mA cm^{-2}	2668 h	8
9	0.5 mAh cm^{-2}	1 mA cm^{-2}	100 h	9
10	0.5 mAh cm^{-2}	1 mA cm^{-2}	200 h	10
11	0.5 mAh cm^{-2}	1 mA cm^{-2}	1500 h	11
12	0.5 mAh cm^{-2}	1 mA cm^{-2}	700 h	12
13	0.5 mAh cm^{-2}	2 mA cm^{-2}	500 h	13
14	0.5 mAh cm^{-2}	3 mA cm^{-2}	167 h	14
15	**0.5 mAh cm^{-2}**	**2 mA cm^{-2}**	**3500 h**	**This work**

Supplementary Movies

Movie S1 *In-situ* OM investigation of the Zn plating process for pristine Zn electrode at 10 mA cm^{-2} for 30 min (speeding-up 180X).

In the video, non-uniform Zn deposits were observed once the current was applied. Zn dendrites were shown after 10 min and they rapidly grew afterwards.

Movie S2 *In-situ* OM investigation of the Zn plating for (002)-Zn electrode at 10 mA cm^{-2} for 30 min (speeding-up 180X).

In the video, dense deposit layer consisting of packed metal crystals was observed during the entire electrochemical deposition process.

References

[1] Hieu LT, So S, Kim IT, et al. Zn anode with flexible β-PVDF coating for aqueous Zn-ion batteries with long cycle life. Chem Eng J, 2021, 411: 128584.

[2] Kang Z, Wu C, Dong L, et al. 3D porous copper skeleton supported zinc anode toward high capacity and long cycle life zinc ion batteries. ACS Sustainable Chem Eng, 2019, 7: 3364-3371.

[3] Cao L, Li D, Deng T, et al. Hydrophobic organic-electrolyte-protected zinc anodes for aqueous zinc batteries. Angew Chem Int Ed, 2020, 59: 19292-19296.

[4] Cao L, Li D, Hu E, et al. Solvation structure design for aqueous Zn metal batteries. J Am Chem Soc, 2020, 142: 21404-21409.

[5] Ma L, Chen S, Li X, et al. Liquid-free all-solid-state zinc batteries and encapsulation-free flexible batteries enabled by in situ constructed polymer electrolyte. Angew Chem Int Ed, 2020, 59: 23836-23844.

[6] Hao J, Li X, Zhang S, et al. Designing dendrite-free zinc anodes for advanced aqueous zinc batteries. Adv Funct Mater, 2020, 30: 2001263.

[7] Verma V, Chan RM, Yang L, et al. Chelating ligands as electrolyte solvent for rechargeable zinc-ion batteries. Chem Mater, 2021, 33: 1330-1340.

[8] Qin R, Wang Y, Zhang M, et al. Tuning Zn2+ coordination environment to suppress dendrite formation for high-performance Zn-ion batteries. Nano Energy, 2021, 80: 105478.

[9] Qiu H, Du X, Zhao J, et al. Zinc anode-compatible in-situ solid electrolyte interphase via cation solvation modulation. Nat Commun, 2019, 10: 5374.

[10] Wang J, Cai Z, Xiao R, et al. A chemically polished zinc metal electrode with a ridge-like structure for cycle-stable aqueous batteries. ACS Appl Mater Interfaces, 2020, 12: 23028-23034.

[11] Cai Z, Ou Y, Wang J, et al. Chemically resistant Cu–Zn/Zn composite anode for long cycling aqueous batteries. Energy Storage Mater, 2020, 27: 205-211.

[12] Cai Z, Ou Y, Zhang B, et al. A replacement reaction enabled interdigitated metal/solid electrolyte architecture for battery cycling at 20 mA cm(-2) and 20 mAh cm(-2). J Am Chem Soc, 2021, 143: 3143-3152.

[13] Cui Y, Zhao Q, Wu X, et al. An interface-bridged organic-inorganic layer that suppresses dendrite formation and side reactions for ultra-long-life aqueous zinc metal anodes. Angew Chem Int Ed, 2020, 59: 16594-16601.

[14] Zhou Y, Wang X, Shen X, et al. 3D confined zinc plating/stripping with high discharge depth and excellent high-rate reversibility. J Mater Chem A, 2020, 8: 11719-11727.